Elsevier Editorial System(tm) for Catalysis Today

Manuscript Draft

Manuscript Number:

Title: Cu/TiO2 photocatalysts for the conversion of acetic acid into biogas and hydrogen

Article Type: SI: Selected papers SPEA-9

Keywords: Photocatalysis; TiO2; copper; degradation; acetic acid; biogas

Corresponding Author: Dr. M. Angeles Lillo, PhD

Corresponding Author's Institution: University of Alicante

First Author: Ana Amoros-Perez

Order of Authors: Ana Amoros-Perez; Laura Cano-Casanova; M. Angeles Lillo, PhD; Mari Carmen Roman-Martinez, Professor

Abstract: Photocatalytic decomposition of acetic acid into biogas and hydrogen was performed over Cu/TiO2 photocatalysts synthesized by the sol-gel method. Samples with different Cu loadings (0, 0.5, 1 and 10 wt. %) were prepared by two different methods (in situ and impregnation), and then they were heat treated at 500 °C either in air or in argon. Structural and surface characterization of the photocatalysts was carried out. The influence of the synthesis variables on their efficiency in the photocatalytic decomposition of acetic acid in aqueous solution was analysed.

The photodegradation results show that all the prepared materials are more active than commercial TiO2 (P25), used as a reference, and reveal that the presence of copper improves the activity of pure TiO2. Cu/TiO2 photocatalysts prepared by the in situ method and heat treated in argon show the best results. This can be explained considering that these synthesis conditions lead to more efficient interaction between Cu species and TiO2, to a more developed porosity and to a more suitable distribution of copper oxidation states (large contribution of Cu(I) and Cu(0) seem to give better activity). Catalysts with 0.5 wt.% copper are the most active, likely because copper species are highly dispersed and interact efficiently with TiO2. Thus, the activity of catalyst Cu/TiO2is0.5-Ar is double than that of the TiO2-P25 commercial catalyst.

HIGHLIGHTS

- The effect of the synthesis variables of Cu/TiO_2 photocatalysts was investigated
- Cu wt%, Cu incorporation method, and heat-treatment atmosphere were analyzed
- Photocatalytic decomposition of acetic acid in aqueous solution was studied
- Methane and hydrogen are the preferred decomposition products
- High surface area, small crystal size and presence of $Cu^{(I)}$ and $Cu^{(0)}$ are desirable

***Graphical Abstract (for review)**

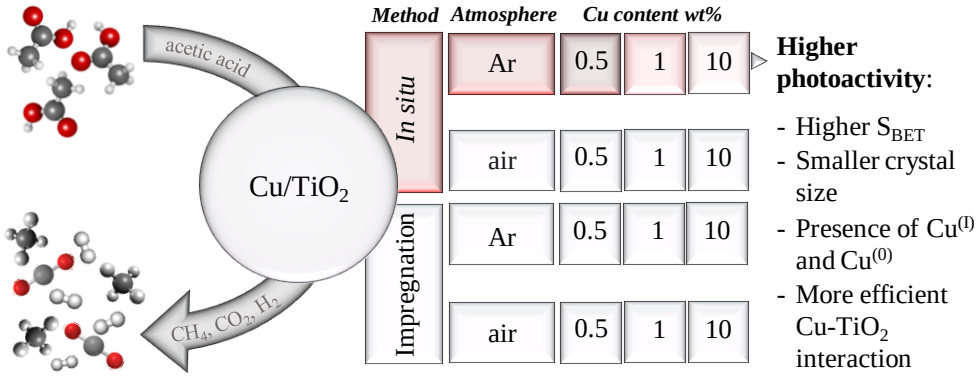

Cu/TiO_2 photocatalysts for the conversion of acetic acid into biogas and hydrogen

Ana Amorós-Pérez, Laura Cano-Casanova, María Ángeles Lillo-Ródenas, M. Carmen Román-Martínez.*

MCMA Group, Department of Inorganic Chemistry and Materials Institute. Faculty of Sciences.

University of Alicante. Ap.99. E-03080 Alicante. SPAIN. (mlillo@ua.es).

Abstract

Photocatalytic decomposition of acetic acid into biogas and hydrogen was performed over Cu/TiO_2 photocatalysts synthesized by the sol-gel method. Samples with different Cu loadings (0, 0.5, 1 and 10 wt. %) were prepared by two different methods (*in situ* and impregnation), and then they were heat treated at 500 ºC either in air or in argon. Structural and surface characterization of the photocatalysts was carried out. The influence of the synthesis variables on their efficiency in the photocatalytic decomposition of acetic acid in aqueous solution was analyzed.

The photodegradation results show that all the prepared materials are more active than commercial TiO_2 (P25), used as a reference, and reveal that the presence of copper improves the activity of pure TiO_2. Cu/TiO_2 photocatalysts prepared by the *in situ* method and heat treated in argon show the best results. This can be explained considering that these synthesis conditions lead to more efficient interaction between Cu species and TiO_2, to a more developed porosity and to a more suitable distribution of copper oxidation states (large contribution of $Cu^{(I)}$ and $Cu^{(0)}$ seem to give better activity). Catalysts with 0.5 wt.% copper are the most active, likely because copper species are highly dispersed and interact efficiently with TiO_2. Thus, the activity of catalyst *Cu/TiO_2is0.5-Ar* is double than that of the TiO_2-P25 commercial catalyst.

Keywords: *Photocatalysis; TiO_2; copper; degradation; acetic acid; biogas*

**Corresponding author. Tel.: +34 965 903545; e-mail: mlillo@ua.es*
Fax: +34 965 903454

1. Introduction

For the past few decades, increased concern about greenhouse gases emissions and depletion of non-renewable resources has contributed to the development of new methods of energy production, mainly from alternative sources such as biomass. Biomass covers a wide range of organic materials of heterogeneous nature, origin and composition, including waste organic materials.

One of the most promising methods of energy production is the transformation of organic substrates to biogas [1,2], a mixture of different gases (mainly methane and carbon dioxide) which is considered an ecological, economic and efficient fuel [3]. The organic matter which contaminates water is transformed into acetic acid due to the presence of microorganisms in the medium and this compound can be converted to biogas by photocatalytic oxidation. Photocatalysis is one of the so-called Advanced Oxidation Technologies (AOTs) and has attracted great interest in recent years [4]. In the presence of a photocatalyst (a semiconducting substance) a chemical reaction can be boosted or initiated under the action of ultraviolet, visible or infrared radiation [5]. If the energy of the irradiation source matches or exceeds that of the photocatalyst band gap (Eg), an electron (e^-) of the valence band (VB) can be excited to the conduction band (CB), leaving a positive hole (h^+) in the VB (Fig. 1). Photogenerated electrons and positive holes drive reduction and oxidation, respectively, of different compounds (Figure 1) [6]. Thus, photocatalysts can act as mediators in chemical redox processes [7].

The efficiency of a photocatalytic process depends on factors such as the recombination rate of photogenerated electron-hole pairs, the incident radiation wavelength, and the crystal size, crystallinity and surface area of the photocatalyst [9,10]. Thus, a photocatalyst must have high surface area, high crystallinity, small crystal size and low electron-hole pairs recombination rate to achieve high photoactivity [11–13].

Titanium dioxide is one of the most widely used photocatalysts due to numerous advantages, such as high thermodynamic stability, resistance to corrosive media, presence of crystalline structures of high activity (anatase and rutile) and relative low cost due to the moderate abundance of titanium on the earth crust [8,14]. However, TiO_2 has some drawbacks. The efficiency is often low due to the fast recombination of

photogenerated holes and electrons (h^+/e^-) and it has a relatively wide band gap (3.2 eV), so it is only active in the near ultraviolet region (UV) [15], which means that only about 5% of the solar radiation can be used.

One of the potential solutions to improve TiO_2 efficiency is to extend its photoresponse from the UV to the visible light region [16]. Such a band reconstruction and band-gap narrowing [17] can be achieved by the introduction of transition metals into the TiO_2 lattice. Generally, the metal species are considered to act as trapping sites, which accept the photogenerated electrons or holes from the TiO_2, and restrain the combination of carriers [18].

Copper oxides have narrow band-gap energies and high light adsorption coefficients, and thus they have been considered suitable to modify TiO_2. Numerous studies have used TiO_2 for the degradation of organic pollutants in aqueous media [19–23], but TiO_2 modified with copper has been scarcely studied [24–27]. So far, Heciak et al. conducted some research on the conversion of acetic acid to hydrocarbons and hydrogen using Cu/TiO_2 photocatalysts prepared with a commercial TiO_2 by different methods and using several Cu precursors [28]. Their results revealed that copper catalysts produced hydrocarbons and hydrogen, but the amount of methane produced was not studied.

Considering this, the aim of this study is to develop Cu/TiO_2 catalysts for the photocatalytic decomposition of acetic acid with the purpose of obtaining methane and hydrogen. Hence, acetic acid has been chosen as a representative biomass compound and starting material for the production of energy. The TiO_2 materials were prepared by sol-gel, and copper was incorporated by two methods, impregnation and *in situ* (during the sol-gel synthesis), using $Cu(NO_3)_2$ aqueous solutions.

2. Materials and methods

2.1. Preparation of TiO_2

Nanosized TiO_2 particles were prepared by sol-gel method using titanium tetraisopropoxide (TTIP) as precursor. The procedure comprises the following steps [29]: 1) 9.3 ml TTIP were mixed with 17.5 ml glacial acetic acid (AcAc) at 0 ºC, 2) 197.5 ml distilled water were added dropwise under vigorous stirring for 1 h (the TTIP:AcAc:H_2O molar ratio was 1:10:350), 3) the solution was ultrasonicated for

30 min, 4) solution stirring continued for 5 h until a clear suspension of TiO_2 nanocrystals was formed, 5) the suspension was aged in an oven at 70 °C for 12 h and, finally 6) the resulting gel was dried at 100 °C and the solid crushed into a fine powder [30]. A certain amount of this TiO_2 was heat treated as specified in section 2.3.

2.2. Synthesis of Cu/TiO_2 samples

2.2.1. *Impregnation (im)*

1 g of dried TiO_2 was put in contact with an aqueous solution of $Cu(NO_3)_2 \cdot 3H_2O$ (5 ml) of the appropriate concentration to obtain Cu loadings of 0.5, 1 and 10 wt.%. The mixture was stirred for 2 h and then the solvent excess was removed by heating at 80 ºC for 24 h. The nomenclature used is *Cu/TiO_2imx* (x= 0.5, 1 or 10). The obtained solids were crushed and heat treated as described in section 2.3.

2.2.2. *In situ (is)*

An aqueous solution of $Cu(NO_3)_2 \cdot 3H_2O$ (5 ml) with the appropriate concentration to obtain Cu loadings of 0.5, 1 and 10 wt.% was introduced dropwise in the step 2 of the TiO_2 sol-gel synthesis. Then, the remaining amount of distilled water (up to 197.5 ml) was added dropwise. The rest of the steps remain as described in part 2.1. The nomenclature for these samples is *Cu/TiO_2isx* (x = 0.5, 1 or 10).

2.3. Heat treatment of the samples

The heat treatment was performed to increase the crystallinity of TiO_2 [31], to remove impurities [32] and to strengthen the metal-TiO_2 interaction [33]. The treatment was carried out in a fixed bed quartz reactor and consisted of a 5 ºC/min heating step, either in air or in Ar (90 ml/min), up to 500 ºC with 2 h soaking time. The samples name includes *Ar* or *air* to indicate the atmosphere of the heat treatment. The calcination temperature, 500 ºC, was selected in order to have a large amount of anatase crystalline phase [31,34].

2.4. Catalysts characterization

The textural properties were characterized by N_2 adsorption at -196 ºC (after degasification at 250 ºC for 4 h) in an Autosorb-6B equipment (Quantachrome). The specific BET surface area (S_{BET}) was determined by applying the Brunauer–Emmett–Teller (BET) equation [35].

The crystallinity was studied by X-ray diffraction (XRD) analysis using Cu Kα (1.54 Å) radiation in a SEIFERT 2002 equipment. The scanning velocity was 2°/min, and diffraction patterns were recorded in the angular 2θ range 6–80º. The average crystallite size, referred to as crystal size, was calculated by the Scherrer's equation [36]:

$$B = \frac{K\lambda}{\beta \cos\theta} \quad (1)$$

where B is the average crystallite size (nm); K is a constant, with a chosen value of 0.9 [37]; λ is the wavelength of the radiation source; β is the full width at half maximum intensity (FWHM) and θ is the Bragg angle of the maximum intensity peak.

XPS spectra were obtained using a K-Alpha spectrophotometer (Thermo-Scientific), with a high resolution monochromator and the following specifications: Al anode (1486.6 eV) X-ray source, 5×10^{-9} mbar analysis chamber pressure and detection in constant energy mode with pass energy of 200 eV for the survey spectrum and of 50 eV for the sweep in each individual region. Data analysis was performed with the Peak-Fit software and binding energy values were adjusted to the C1s transition (284.6 eV).

A CuO sample obtained by calcination of $Cu(NO_3)_2 \cdot 3H_2O$ using a 10 ºC/min heating rate up to 500 ºC held for 1 h was analyzed and used as reference.

2.5. Photocatalytic measurements

Photocatalytic tests were performed in a cylindrical quartz reactor (Heraeus, type UV-RS-2). The light source is a medium pressure mercury vapor lamp (TQ-150, λ_{max} = 365 nm) located in the center of the vessel and surrounded by a water circulating jacket. Gas inlet and outlet are located in the upper part of the reactor.

In a typical experiment, 0.35 ml of 1M CH_3COOH aqueous solution and 0.35 g of photocatalyst were introduced in the reactor. Then, a stream of He (60 mL/min) was bubbled through the reactor for 2 h to purge lines and to remove dissolved oxygen, and afterwards the cooling system and the UV lamp were turned on to start the photoreaction. The process was conducted for 12 h under continuous magnetically stirring. Some experiments were repeated twice in order to check for reproducibility.

The outlet gas stream was fed to a mass spectrometer (Balzers, Thermostar GSD 301 01) to analyze CH_4, CO_2 and H_2 produced.

The photocatalytic activity was expressed as CH_4, CO_2 and H_2 production, calculated as shown in eq. 2.

$$\text{Production of x} = \frac{\text{mmol x}}{\text{mol AcAc} \cdot \text{g catalyst}} \quad (2)$$

Where x is CH_4, CO_2 or H_2.

3. Results and discussion

3.1. Porosity characterization

Table 1 summarizes the BET surface areas of the photocatalysts prepared and of the commercial TiO_2-P25 (Evonik). It can be observed that the surface area of the synthesized TiO_2 is larger than that of P25, and sample *TiO_2-air* has slightly higher surface area than *TiO_2-Ar*. Likely, air causes the oxidation of some impurities present in the material and favors the conversion of unreacted TTIP to TiO_2. Comparing Cu/TiO_2 samples with TiO_2 treated in the same atmosphere, it can be observed that most Cu/TiO_2-Ar samples have slightly larger surface area than *TiO_2-Ar*. Contrarily, all Cu/TiO_2-air samples have lower surface area than *TiO_2-air*, possibly because the heat treatment in air could transform more effectively the Cu precursor into Cu oxides, with lower surface area, and/or could block some porosity. For the same reason, Cu/TiO_2-Ar samples have larger surface area than Cu/TiO_2-air samples (with the exception of *Cu/TiO_2im10*).

Comparing samples with different Cu loading it can be observed that, in general, the surface areas decrease when the Cu contents increase. For Cu/TiO_2 samples prepared with 0.5 or 1 wt.% Cu, the heat treatment in argon leads to more developed surfaces than the treatment in air, and the method used for the incorporation of copper, either impregnation or in-situ, has no effect in terms of porosity. In the case of samples that contain 10 wt.% Cu tendencies are not so clear, being sample *Cu/TiO_2 is10-Ar* the one with the largest surface area.

3.2. XRD analysis

The obtained XRD patterns (Figure 2) show the peaks corresponding to anatase (25.3º ((101) plane), 37.8º ((004) plane), 48.0º ((200) plane), 53.9º ((105) plane) 55.1º ((211) plane), 62.7º ((204) plane), 70.4º ((116) plane) and 74.5º ((220) plane) [39,40]),

while no rutile peaks are found. This confirms that the heat treatment at 500 ºC leads to the desired TiO_2 phase.

Table 1 shows that the crystal size of all the samples synthesized is smaller than that of P25. Regarding the effect of the synthesis variables, it can be observed that: i) except in the case of samples with 10 wt.% Cu, the heat treatment in air leads to larger crystal sizes than the treatment in Ar and ii) Cu/TiO_2 samples have larger crystal sizes than their corresponding heat-treated TiO_2 samples. Therefore, the presence of copper has an influence on the development of the crystal structure. In this sense, literature states that the formation of CuO likely generates a large number of defects as oxygen vacancies in the TiO_2 network, which act as nuclei for new crystals, accelerating the crystallization process and leading to larger crystals [41].

The obtained XRD patterns do not show any characteristic peaks of copper oxides (which would appear at 2 theta values: 36.65º and 61.36º for Cu_2O cuprite [42], and 35.75º and 38.95º for the tenorite structure CuO [43,44]). Only sample *Cu/TiO₂is10-Ar* presents peaks corresponding to metallic copper (2 theta values: 43.47º, 50.69º and 74.67º for face-cubic centered $Cu^{(0)}$ [45]), whereas this peak is not observed in samples *Cu/TiO₂is0.5-Ar* and *Cu/TiO₂is1-Ar*, prepared in the same way but with a much lower Cu content. This can be explained considering that the low $Cu^{(0)}$ content in these samples and its high dispersion leads to not observable $Cu^{(0)}$ XRD peaks in *Cu/TiO₂is0.5-Ar* and *Cu/TiO₂is1-Ar*. To check this point, three additional samples, *Cu/TiO₂is2-Ar*, *Cu/TiO₂is5-Ar* and *Cu/TiO₂is7-Ar*, were prepared and characterized by XRD. The obtained results reveal the presence of metallic copper and do not show patterns corresponding to copper oxides. Considering this, we assume that all *Cu/TiO₂isx-Ar* photocatalysts contain $Cu^{(0)}$, even those with 0.5 or 1 wt.% Cu, although it is not observed by XRD due to the low Cu loading and/or the high Cu dispersion [43].

3.3. XPS characterisation

Figure 3 shows the Cu $2p_{3/2}$ spectra obtained for the different Cu/TiO_2 photocatalysts and for the CuO reference. The $2p_{3/2}$ level of CuO is characterized by a shake-up satellite peak due to multiplet splitting that appears at a binding energy about 9 eV higher than the $2p_{3/2}$ peak [14,46]. The satellite peak arises when the emitted photoelectron loses part of its kinetic energy to excite a valence electron to an unoccupied d orbital of Cu. The presence of the satellite peak is, therefore, an indication

of the existence of d^9 partially filled orbitals in Cu fundamental state and thus, it appears only when $Cu^{(II)}$ species are present.

The XPS spectrum of the CuO reference presents a main signal located at 933.7 eV and the satellite peak, previously described, presents two maxima at 941.3 and 943.8 eV, in agreement with the presence of $Cu^{(II)}$. For the 10 wt.% Cu/TiO_2 catalysts the satellite peak is also observed, but the main signal can be deconvoluted into two contributions, indicating different oxidation states of copper. The contribution at higher binding energycan be assigned to $Cu^{(II)}$ and the one at lower B.E. values can be assigned to $Cu^{(I)}$ (B.E 932.1 eV [47]) and/or to $Cu^{(0)}$ (B.E 932.4 eV [48]). Thus, the information provided by these two contributions of the main Cu $2p_{3/2}$ peak is of great interest: it indicates the presence of $Cu^{(I)}$ in samples that, according to XRD, do not contain $Cu^{(0)}$. However, in samples in which XRD data reveal the presence of $Cu^{(0)}$, $Cu^{(I)}$ species can be neither confirmed nor discarded. In the case of catalysts with 0.5 and 1 wt.% Cu loadings, the satellite peak is almost not observed because the signal intensity is very low, but the fact that the main peak shows two contributions seems to indicate that these samples also contain copper in different oxidation states. Therefore, $Cu^{(II)}$ and $Cu^{(I)}$ species coexist in most samples. $Cu^{(0)}$ is only present in samples prepared by *in situ* method and treated in Ar. Thus, *$Cu/TiO_2$is-Ar* samples certainly contain $Cu^{(II)}$ and $Cu^{(0)}$ and, possibly $Cu^{(I)}$, although as mentioned before the presence of $Cu^{(I)}$ cannot be neither confirmed nor discarded considering our experimental data.

The amount of $Cu^{(II)}$ in the different samples was determined by the method reported by Biesinger et al. [38]. Data included Table 1 show that all samples contain $Cu^{(II)}$. Comparison of the $Cu^{(II)}$ content shows that, in general, samples prepared *in situ* and treated in Ar contain a lower $Cu^{(II)}$ percentage. Comparing the different preparation conditions, samples with lower $Cu^{(II)}$ percentage are *$Cu/TiO_2$is-Ar* ones and, generally, increasing Cu loading increases the $Cu^{(II)}$ percentage. Thus, it is also worth mentioning that the $Cu^{(II)}$ percentage in samples with 0.5 wt.% Cu is very low.

3.4. Study of the photocatalytic activity

Figure 4 compiles the photocatalytic activity results obtained with P25, TiO_2 and 0.5 wt.% Cu/TiO_2 samples. It shows that the prepared photocatalysts are more active than P25, in agreement with their larger surface areas and lower crystal sizes. *TiO_2-air* is more active than *TiO_2-Ar* but, on the contrary, Cu/TiO_2-Ar catalysts are more active

than Cu/TiO_2-air. According to these data, the higher activity can be related with the larger surface areas, which are also related with crystal sizes (note that for a similar crystalline phase contents the lower the crystal sizes, the larger the surface areas).

Regarding the preparation method, *Cu/$TiO_2$is* catalysts are more active than *Cu/TiO_2im*, although they have similar surface areas and crystal sizes (Table 1). These results emphasize that the activity depends on a combination of properties including surface area, crystallinity and crystal size, but other parameters such as copper-TiO_2 interaction and the distribution of copper oxidation states seem to play a relevant role. Thus, the different activity of samples prepared by impregnation or *in situ* methods could be due to a different interaction between Cu species and TiO_2, being this probably more effective in the *is*-samples. On the other hand, samples treated in Ar are more active than those prepared in air, and this could be attributed to a more suitable composition/content of the more photocatalytically active oxidation states of copper.

Sample *Cu/TiO_2is0.5-Ar* is the most active one (Figure 4). Compared to other samples with the same Cu loading, it contains the lowest $Cu^{(II)}$ percentage (Table 1), and possibly contains some $Cu^{(0)}$ and $Cu^{(I)}$, which may be beneficial for the photocatalytic process. Considering this, it can be concluded that the best preparation conditions imply the *in situ* method to incorporate Cu and heat treatment in Ar.

In order to analyze the effect of the copper loading, the activities of *Cu/TiO_2isx-Ar* catalysts with 0.5, 1 and 10 wt.% Cu are compared in Figure 5. It can be observed that an increase in the copper content leads to a reduction in the amount of H_2, CO_2 and CH_4 produced. Note that with the Cu content increase, the surface areas of these samples decrease and their crystal sizes increase. In addition, lower Cu loading could be related to a higher metal dispersion, as reported in the literature [49] and, according to XPS data, increasing the Cu loading increases the $Cu^{(II)}$ percentage. Both aspects seem to be detrimental from the photocatalytic point of view.

Thus, our results show that the coexistence of the three copper oxidation states: $Cu^{(0)}$, $Cu^{(I)}$ and $Cu^{(II)}$, improves the photocatalytic efficiency. This can be explained considering that $Cu^{(I)}$ and $Cu^{(0)}$ can give electrons to the oxygen absorbed on the surface of catalyst, thus accelerating the interfacial electron transfer [47], and $Cu^{(II)}$ can trap excited electrons in conduction band, inhibiting the electron/hole pair recombination.

However, $Cu^{(I)}$ and $Cu^{(0)}$ species have proved to be more relevant than $Cu^{(II)}$, in agreement with previous studies [50].

In order to ensure the reproducibility of the obtained results, in several cases two activity tests were performed, each one with a different portion of sample. Figure 5 shows the production of CH_4, CO_2 and H_2 in two different tests, what reveals that the catalytic experiments performed are highly reproducible.

3. Conclusions

Cu/TiO_2 catalysts with different copper contents (0.5, 1 and 10 wt.%) have been synthesized by sol-gel, using impregnation and *in situ* methods to incorporate copper, and they have been submitted to a heat treatment at 500 °C, either in air or in argon. These catalysts have been tested in the photocatalytic decomposition of acetic acid.

Textural and chemical properties, and photoactivity have been compared with those of pure TiO_2 samples also submitted to the mentioned heat treatments.

The prepared photocatalysts are more active than commercial TiO_2-P25 in the decomposition of acetic acid. The photocatalytic efficiency depends on several parameters. Among them, surface area, crystal phase and crystallite size have a very important effect. Furthermore, the presence of copper plays an important role, and most copper-containing samples are more active than pure TiO_2 samples. Cu/TiO_2 samples synthetized by *in situ* method and heat treated in argon give rise to the best photocatalytic efficiency. The most active sample is *Cu/TiO₂is0.5-Ar*, the one with one of the largest surface areas, relatively small crystal size, the lowest $Cu^{(II)}$ percentage and that likely contains highly-dispersed copper species.

These results remark the importance of the interaction between copper and titanium dioxide and the distribution of the copper oxidation states on the photocatalytic activity. Considering all this, it can be concluded that in order to improve photocatalytic activity for this application a photocatalyst should combine several characteristics: high surface area, small crystal size, highly dispersed copper with an efficient interaction with TiO_2 and a suitable distribution of copper species, being interesting high percentages of $Cu^{(I)}$ and $Cu^{(0)}$ species.

4. Acknowledgements

The authors thank funding to the Spanish Ministry of Economy and Competitiveness (MINECO) and FEDER, project of reference CTQ2015-66080-R, GV/FEDER (PROMETEOII/2014/010) and University of Alicante (VIGROB-136) for financial support.

5. References

[1] B. Demirel, P. Scherer, Renew. Energy. 34 (2009) 2940–2945.

[2] M. Pöschl, S. Ward, P. Owende, Appl. Energy. 87 (2010) 3305–3321.

[3] S. Mozia, Int. J. Photoenergy. 2009 (2009).

[4] M.I. Litter, R.J. Candal, J.M. Meichtry, Avanced Oxidation Technologies: sustainable solutions for environmental treatments, frist ed., CRC Press, Netherlands, 2014.

[5] S.E. Braslavsky, A.M. Braun, A.E. Cassano, A. V. Emeline, M.I. Litter, L. Palmisano, et al., Pure Appl. Chem. 83 (2011) 931–1014.

[6] U.I. Gaya, A.H. Abdullah, J. Photochem. Photobiol. C Photochem. Rev. 9 (2008) 1–12.

[7] D. Spasiano, R. Marotta, S. Malato, P. Fernandez-Ibanez, I. Di Somma, Appl. Catal. B Environ. 170 (2015) 90–123.

[8] K. Nakata, A. Fujishima, J. Photochem. Photobiol. C Photochem. Rev. 13 (2012) 169–189.

[9] S. Sahni, S.B. Reddy, B.S. Murty, Mater. Sci. Eng. A. 452-453 (2007) 758–762.

[10] Z. Zhang, C.-C. Wang, R. Zakaria, J.Y. Ying, J. Phys. Chem. B. 102 (1998) 10871–10878.

[11] S.-J. Tsai, S. Cheng, Catal. Today. 33 (1997) 227–237.

[12] J.F. Porter, Y.G. Li, C.K. Chan, J. Mater. Sci. 34 (1999) 1523–1531.

[13] H.D. Jang, S. Kim, S. Kim, J. Nanoparticle Res. 3 (2001) 141–147.

[14] M.F. Al-Kuhaili, Vacuum. 82 (2008) 623–629.

[15] M. Anpo, J. Catal. 216 (2003) 505–516.

[16] X. Yue, S. Jiang, L. Ni, R. Wang, S. Qiu, Z. Zhang, Chem. Phys. Lett. 615 (2014) 111–116.

[17] H. Tong, S. Ouyang, Y. Bi, N. Umezawa, M. Oshikiri, J. Ye, Adv. Mater. 24 (2012) 229–51.

[18] M.A. Barakat, H. Schaeffer, G. Hayes, S. Ismat-Shah, Appl. Catal. B Environ. 57 (2005) 23–30.

[19] M. Yasmina, K. Mourad, S.H. Mohammed, C. Khaoula, Energy Procedia. 50 (2014) 559–566.

[20] R.A. Torres, J.I. Nieto, E. Combet, C. Pétrier, C. Pulgarin, Appl. Catal. B Environ. 80 (2008) 168–175.

[21] S. Murgolo, F. Petronella, R. Ciannarella, R. Comparelli, A. Agostiano, M.L. Curri, et al., Catal. Today. 240 (2015) 114–124.

[22] I. Nitoi, P. Oancea, I. Cristea, L. Constsntin, G. Nechifor, J. Photochem. Photobiol. A Chem. 298 (2015) 17–23.

[23] S. Asal, M. Saif, H. Hafez, S. Mozia, A. Heciak, D. Moszyński, et al., Int. J. Hydrogen Energy. 36 (2011) 6529–6537.

[24] C. He, D. Shu, M. Su, D. Xia, L. Lin, Y. Xiong, Desalination. 253 (2010) 88–93.

[25] H.W.P. Carvalho, A.P.L. Batista, P. Hammer, T.C. Ramalho, J. Hazard. Mater. 184 (2010) 273–80.

[26] L.-F. Chiang, R.-A. Doong, J. Hazard. Mater. 277 (2014) 84–92.

[27] J.F. Góngora-Gómez, P. Elizondo-Martínez, N. Pérez, M. Villanueva-Rodríguez, L. Hinojosa-Reyes, A. Hernández-Ramírez, Ceram. Int. 40 (2014) 14207–14214.

[28] A. Heciak, A.W. Morawski, B. Grzmil, S. Mozia, Appl. Catal. B Environ. 140-141 (2013) 108–114.

[29] M. Ouzzine, M.A. Lillo-Ródenas, A. Linares-Solano, Appl. Catal. B Environ. 134-135 (2013) 333–343.

[30] N. Venkatachalam, M. Palanichamy, V. Murugesan, Mater. Chem. Phys. 104 (2007) 454–459.

[31] Y. Tanaka, M. Suganuma, J. Sol-Gel Sci. Technol. 22 (2001) 83–89.

[32] G. Colón, M. Maicu, M.C. Hidalgo, J.A. Navío, Appl. Catal. B Environ. 67 (2006) 41–51.

[33] V.G. Deshmane, S.L. Owen, R.Y. Abrokwah, D. Kuila, J. Mol. Catal. A Chem. 408 (2015) 202–213.

[34] D. Fang, Z. Luo, K. Huang, D.C. Lagoudas, Appl. Surf. Sci. 257 (2011) 6451–6461.

[35] S. Brunauer, P.H. Emmett, E. Teller, J. Am. Chem. Soc. 60 (1938) 309–319.

[36] H. Zhang, J.F. Banfield, J. Phys. Chem. B. 104 (2000) 3481–3487.

[37] P. Praveen, G. Viruthagiri, S. Mugundan, N. Shanmugam, Spectrochim. Acta. A. Mol. Biomol. Spectrosc. 117 (2014) 622–9.

[38] M.C. Biesinger, L.W.M. Lau, A.R. Gerson, R.S.C. Smart, Appl. Surf. Sci. 257 (2010) 887–898.

[39] Y.M. Shul'ga, D. V. Matyushenko, E.N. Kabachkov, a. M. Kolesnikova, E.N. Kurkin, I. a. Domashnev, et al., Tech. Phys. 55 (2010) 141–143.

[40] T. Aguilar, J. Navas, R. Alcántara, C. Fernández-Lorenzo, J.J. Gallardo, G. Blanco, et al., Chem. Phys. Lett. 571 (2013) 49–53.

[41] M.S.P. Francisco, V.R. Mastelaro, Chem. Mater. 14 (2002) 2514–2518.

[42] F. Niu, Y. Jiang, W. Song, Nano Res. 3 (2010) 757–763.

[43] K.-H. Kim, S.-K. Ihm, J. Hazard. Mater. 146 (2007) 610–6.

[44] Z. Wang, Q. Liu, J. Yu, T. Wu, G. Wang, Appl. Catal. A Gen. 239 (2003) 87–94.

[45] K. Rahman, A. Khan, N.M. Muhammad, J. Jo, K.-H. Choi, J. Micromechanics Microengineering. 22 (2012) 065012.

[46] J. Morales, L. Sánchez, F. Martín, J.R. Ramos-Barrado, M. Sánchez, Thin Solid Films. 474 (2005) 133–140.

[47] W. Shu-Xin, M. Zhi, Q. Yong-Ning, H. Fei, J. Li-Shan, Z. Yan-Jun, Phys. Chim. Sin. 19 (2003) 967–969.

[48] Y. Lv, X. Cao, H. Jiang, W. Song, C. Chen, J. Zhao, Appl. Catal. B Environ. 194 (2016) 150–156.

[49] S. Obregón, M.J. Muñoz-Batista, M. Fernández-García, A. Kubacka, G. Colón, Appl. Catal. B Environ. 179 (2015) 468–478.

[50] L. Huang, F. Peng, F.S. Ohuchi, Surf. Sci. 603 (2009) 2825–2834.

Table 1. Main textural parameters, binding energy (Cu $2p_{3/2}$) and $Cu^{(II)}$ amount.

Sample	S_{BET} (m^2/g)	Anatase crystal size (nm)	Cu $2p_{3/2}$ B.E (eV)		$Cu^{(II)}$ amount* (%)
			CuO contribution	Cu_2O and/or Cu contribution	
P25	60	22.01	-	-	-
TiO_2 -Ar	139	8.25	-	-	-
TiO_2 -air	150	8.85	-	-	-
Cu/TiO_2 im0.5-Ar	154	8.45	934.1	932.2	0.26
Cu/TiO_2 im0.5-air	127	10.28	934.0	932.0	0.21
Cu/TiO_2 is0.5-Ar	153	8.41	934.1	932.1	0.14
Cu/TiO_2 is0.5-air	125	9.76	933.8	932.0	0.26
Cu/TiO_2 im1-Ar	161	7.88	933.0	932.0	25.85
Cu/TiO_2 im1-air	104	10.50	933.8	931.9	55.65
Cu/TiO_2 is1-Ar	150	8.90	933.0	931.9	15.10
Cu/TiO_2 is1-air	135	9.13	933.3	931.9	0.72
Cu/TiO_2 im10-Ar	15	19.91	934.4	932.6	46.58
Cu/TiO_2 im10-air	92	9.78	934.4	932.4	29.55
Cu/TiO_2 is10-Ar	130	9.72	934.3	932.4	25.26
Cu/TiO_2 is10-air	84	10.20	934.5	932.5	30.33
CuO	-	-	933.7	-	-

* Determined by the method reported by Biesinger et al. from XPS data [38].

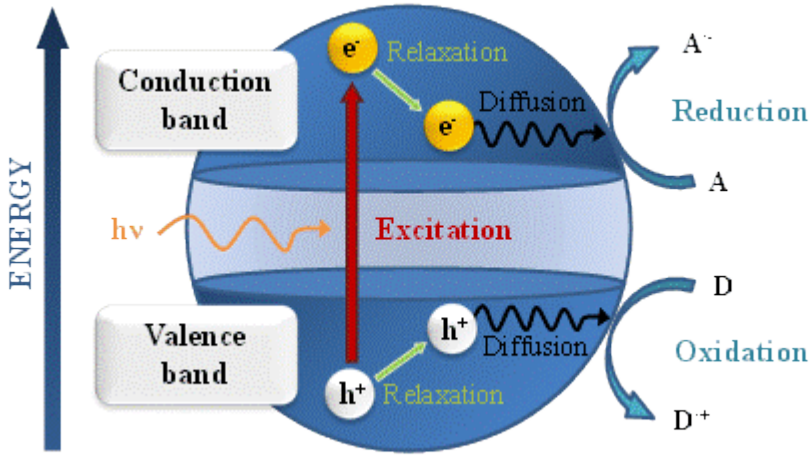

Fig. 1. Schematic illustration of the formation of photogenerated charge carriers (holes and electrons) upon absorption of radiation [8].

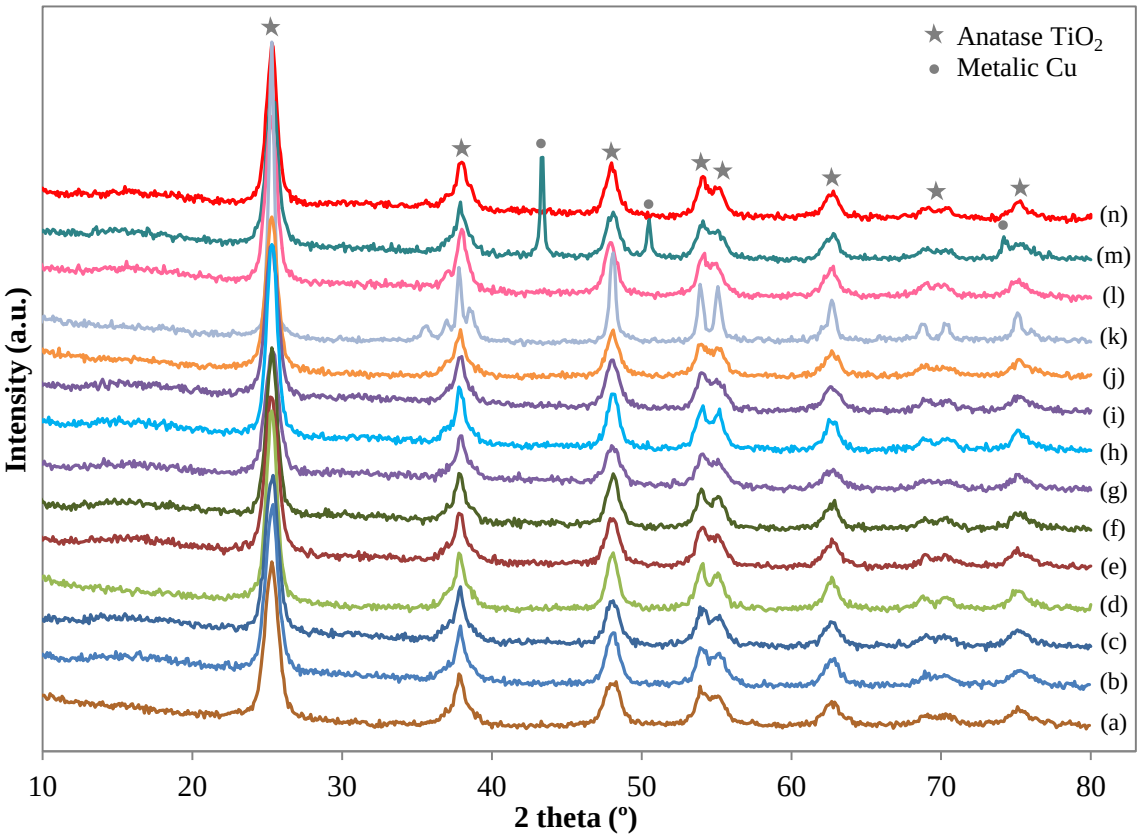

Fig. 2. XRD diffractograms of the synthesized photocatalysts: a) *TiO_2-Ar*, b) *TiO_2-air*, and Cu/TiO_2 samples: c) *im0.5-Ar*, d) *im0.5-air*, e) *is0.5-Ar*, f) *is0.5-air*, g) *im1-Ar*, h) *im1-air*, i) *is1-Ar*, j) *is1-air*, k) *im10-Ar*, l) *im10-air*, m) *is10-Ar* and n) *is10-air*.

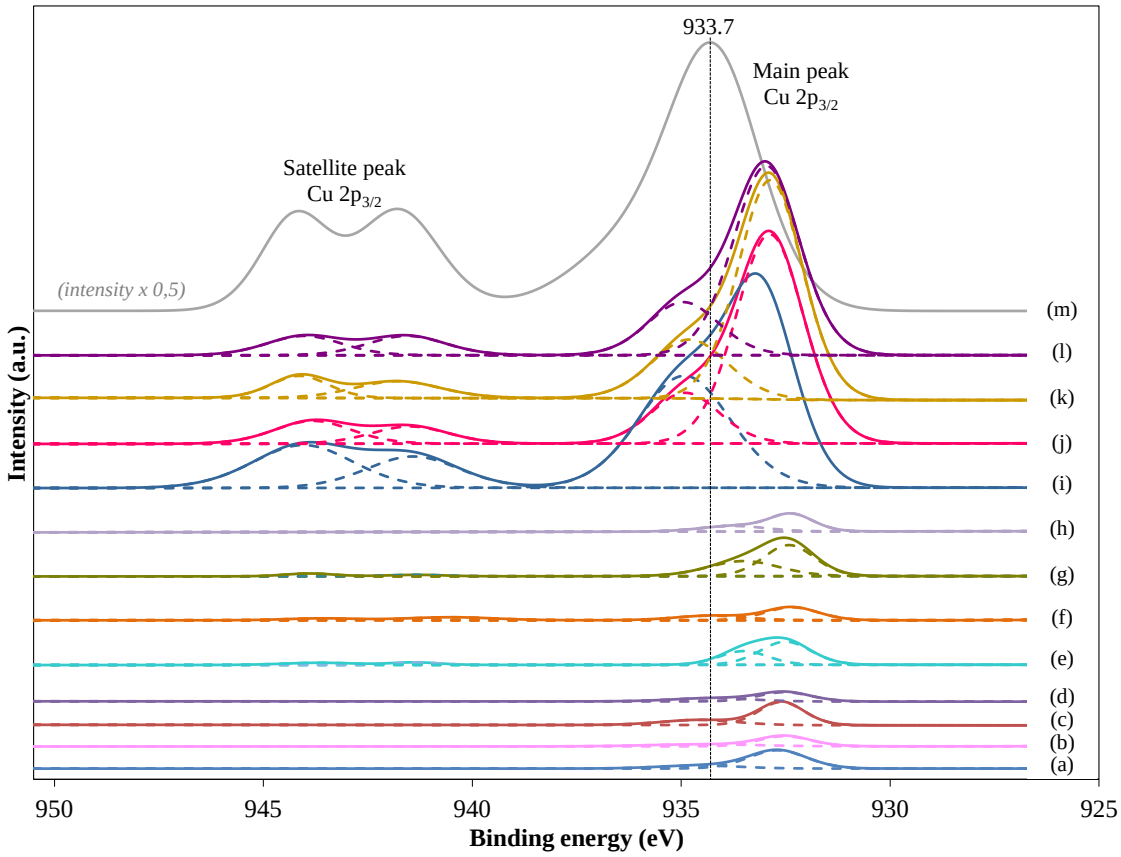

Fig. 3. Cu $2p_{3/2}$ deconvoluted spectra of the Cu/TiO_2 samples: a) *im0.5-Ar*, b) *im0.5-air*, c) *is0.5-Ar*, d) *is0.5-air*, e) *im1-Ar*, f) *im1-air*, g) *is1-Ar*, h) *is1-air*, i) *im10-Ar*, j) *im10-air*, k) *is10-Ar*, l) *is10-air*; and CuO reference (m).

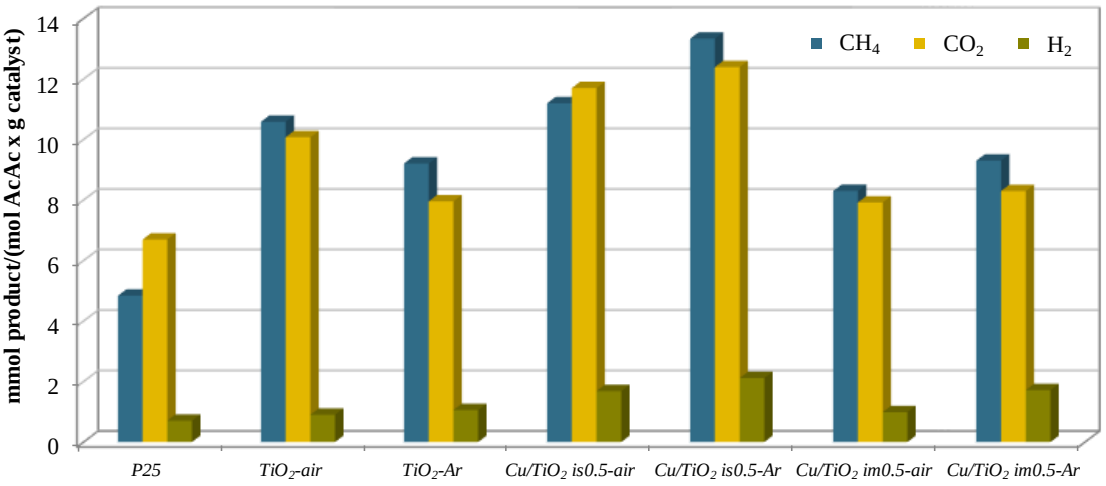

Fig. 4. CH_4, CO_2 and H_2 produced after 12 h in the presence of different photocatalysts.

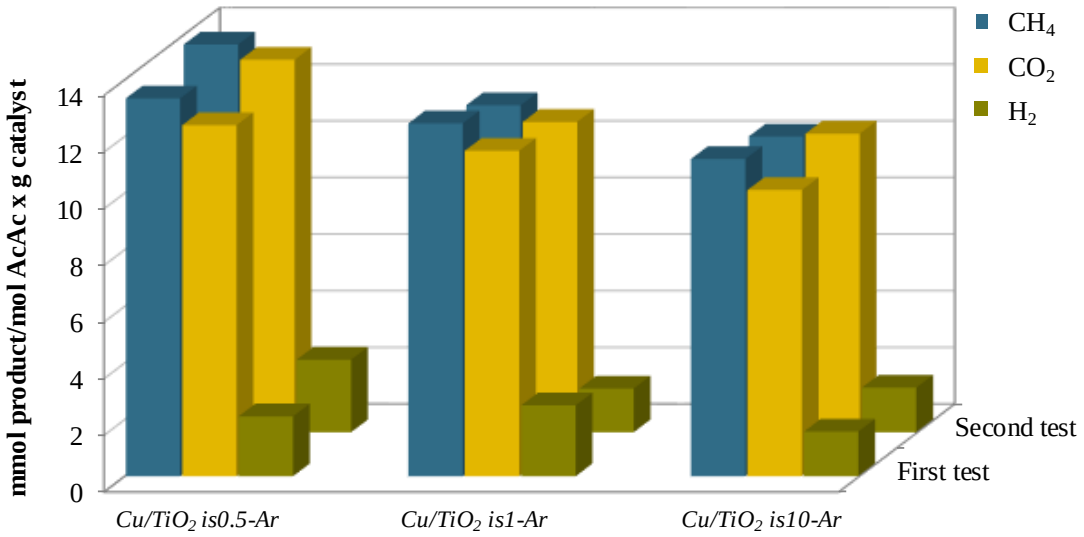

Fig. 5. Produced CH_4, CO_2 and H_2 after 12 h in the presence of *isx-Ar* (x= 0.5, 1, 10) catalysts in two photocatalytic tests.